RSC Advances

PAPER

View Article Online
View Journal | View Issue

Cite this: *RSC Adv.*, 2019, **9**, 39180

Enhanced sodium ion conductivity in Na_3VS_4 by P-doping

Yu He,[a] Fengqi Lu *[b] and Xiaojun Kuang [ab]

Received 29th October 2019
Accepted 22nd November 2019

DOI: 10.1039/c9ra08900d

rsc.li/rsc-advances

All-solid-state sodium-ion batteries are promising candidates for renewable energy storage applications, owing to their high safety, high energy density, and the abundant resources of sodium. The critical factor for an all-solid-state battery is having a sodium solid electrolyte that has high Na ion conductivity at room temperature and outstanding thermal stability, low flammability, and long battery lifespan. Herein, a new Na ion solid-state electrolyte, Na_3VS_4, is prepared by a solid state reaction. It shows conductivity of ~1.16 × 10^{-8} to 1.46 × 10^{-6} S cm^{-1} from 25 to 100 °C. The sodium ion conductivity was enhanced to ~1.49 × 10^{-7} to 1.20 × 10^{-5} S cm^{-1} through P substitution for V in the composition $Na_3P_{0.1}V_{0.9}S_4$. Such sodium ion conduction enhancement could be attributed to P substitution for V leading to a wider Na migration path and the generation of sodium vacancies.

Introduction

There is growing demand for high performance rechargeable batteries used in large-scale energy storage, including electric vehicles and backup storage at individual houses and large-scale solar and wind farms.[1] To date, rechargeable battery technology is dominated by lithium ion batteries, but the geographically constrained Li resources will ultimately push up prices, in turn limiting their application potential in large-scale energy storage. Moreover, from a battery producer viewpoint, principal importance is always given to material abundance and low cost when designing an electrode, *i.e.*, sodium, which is an abundant element in nature while lithium is not. As one classic ion battery, the sodium ion battery has risen to prominence as a key supplement for large-scale energy storage systems.[2] However, severe safety issues also exist in sodium ion batteries using organic liquid electrolytes, because of extremely high reactivity of volatile sodium metal and flammable organic liquid electrolytes.[3–6] Among various methods for improving the safety of electrolytes, the inorganic solid electrolytes have been proposed for development of thermally stable electrolytes.[7] Compared with traditional organic electrolytes, solid state electrolytes have excellent thermal stability,[8] low flammability, and potentially better battery life due to the increased electrochemical stability.[9,10] Based on these advantages, solid-state electrolytes are considered to the most promising components for next generation secondary batteries.

Sulfur-based Na-ion solid electrolytes offer promising room temperature conductivities. The tetragonal phase of Na_3PS_4 had been known as a sodium conductor for more than 20 years.[11] Na_3PS_4 has gained renewed attention since Hayashi *et al.* synthesized a room temperature stable glass–ceramic phase, which showed a Na ionic conductivity of 2 × 10^{-4} S cm^{-1} and subsequently increased to 4.6 × 10^{-4} S cm^{-1} by using high purity raw materials.[12–15] The conductivity of $(1 - x)c$–$Na_3PS_{4-x}Na_4SiS_4$ pseudo-binary system could achieve as high as 7.4 × 10^{-4} S cm^{-1} at x around 0.0629.[16,17] The Cl-doped tetragonal Na_3PS_4 (ref. 18) (t-$Na_{2.9375}PS_{3.9375}Cl_{0.0625}$) solid electrolyte displayed a Na ion conductivity exceeded 1 × 10^{-3} S cm^{-1} at room-temperature. Moreover, the cell parameters had played an important role for Na ion transport, such as Na_3PSe_4 (ref. 19) and Na_3SbS_4,[20] which owned larger cell parameters than Na_3PS_4, their ionic conductivity increased to 1.16 × 10^{-3} S cm^{-1} and 3 × 10^{-3} S cm^{-1}, respectively. Recently, Luo and Wang reported a Na-ion solid-state electrolyte of $Na_3P_{0.62}As_{0.38}S_4$,[21] which had a high ionic conductivity of 1.46 × 10^{-3} S cm^{-1}. Richards *et al.* reported a family of $Na_{10}MP_2S_{12}$ (M = Sn, Ge, and Si) with a high ionic conductivity of 4 × 10^{-4} S cm^{-1} for $Na_{10}SnP_2S_{12}$, and also predicted a super high ionic conductivity of 10.28 × 10^{-3} S cm^{-1} for $Na_{10}SiP_2S_{12}$ based on first-principles simulations.[22,23] Nonetheless, the sodium superionic conductors are still rate and their room-temperature ionic conductivities can't satisfy the actual needs. Looking for new solid-state sodium ion conductor is highly anticipated for all-solid-state rechargeable sodium ion batteries.

Na_3VS_4 crystals were reported more than twenty years ago,[24] which adopted a tetragonal structure closely related to the Na_3PS_4.[11] However, there is no attention on its sodium ionic conductivity so far. In this study, Na_3VS_4 was synthesized by solid state method, which owns sodium ionic conductivity of

[a]*College of Chemistry and Bioengineering, Guilin University of Technology, Guilin 541004, P. R. China*

[b]*Guangxi Key Laboratory of Optical and Electronic Materials and Devices, MOE Key Laboratory of New Processing Technology for Nonferrous Metal and Materials, College of Materials Science and Engineering, Guilin University of Technology, Guilin 541004, P. R. China. E-mail: lufengqi@glut.edu.cn*

$\sim 1.16 \times 10^{-8}$ to 1.46×10^{-6} S cm^{-1} from 25 °C to 100 °C. In order to improve its sodium ionic conductivity, P-doped Na_3VS_4 (*i.e.* $Na_3P_xV_{1-x}S_4$, $0 \leq x \leq 0.2$) was prepared, which resulted in higher Na-ion conductivity of $\sim 1.49 \times 10^{-7}$ to 1.20×10^{-5} S cm^{-1} from 25 °C to 100 °C on composition $x = 0.1$.

Experimental section

Synthesis

$Na_3P_xV_{1-x}S_4$ ($0 \leq x \leq 0.2$) electrolytes were prepared by solid-state reaction in vacuum. The stoichiometric amounts of Na_2S (Aladdin, >95%), P_2S_5 (Aladdin, 99%), and V (Aladdin, 99.99%) were well-mixed and ground with an agate mortar and pestle for one hour. Then, the mixture powder was vacuum-sealed in a quartz tube and heated at 500 °C for 6 h with a heating or cooling rate of 2 °C min^{-1}. All the processes were carried out in a high purity argon-filled glove box with H_2O and O_2 below 0.1 ppm.

Materials characterization

The X-ray diffraction (XRD) data of as-synthesized samples were collected using a PANalytical X'pert Powder X-ray diffractometer equipped with a Cu Kα radiation operating at an accelerating voltage of 40 kV and current of 40 mA. For Rietveld refinement, the data was acquired in the 2θ range of 10–80° with 0.2028° min^{-1}. For all the XRD measurements, to avoid any undesirable influence of air exposure, the as-obtained powders were sealed in an air-tight container with Kapton tape in an argon-filled glove box. The Rietveld refinements of the XRD data were carried out using Topas-Academic software.[25] Raman scattering measurements were performed using DXR Raman Microscope with a 532 nm excitation source. In order to avoid any undesirable influence of air exposure, the as-obtained powders were sealed in an air-tight quartz box.

Electrochemical tests

The alternate current (AC) impedance spectroscopy measurements were performed by using a Solartron SI1260 impedance/gain-phase analyzer over a temperature range from 25 to 100 °C and a frequency range from 10^6 to 10^{-1} Hz. The pellets (φ 6 mm) for AC impedance spectroscopy measurements were pressed from powders at 1000 MPa. The density of the pressed pellet was about 2.14 g cm^{-3}, and achieved a theoretical density of 90%. Platinum foil was placed on both sides of the pellets as electrodes and current collectors. Platinum wire were attached to both sides as current collectors in a cell. The electrochemical stability of as-obtained sample with metallic sodium was determined *via* linear sweep voltammograms (LSV) of the Na/Na_3VS_4/Pt and Na/$Na_3P_{0.1}V_{0.9}S_4$/Pt cells at a scan rate of 0.2 mV s^{-1} from 1 to 6 V at room temperature. To determine electronic conductivity, potentiostatic direct current (DC) polarization measurements were performed on Pt/Na_3VS_4/Pt and Pt/$Na_3P_{0.1}V_{0.9}S_4$/Pt cells by using a Solartron SI1287 electrochemical interface at 25 °C.

Results and discussion

The crystalline phase of as-synthesized samples by solid-state reaction were characterized by XRD. The XRD patterns were shown in Fig. 1, the halo patterns from 10° to 30° reflected from the polyimide film. As shown in Fig. 1a, the major diffraction peaks of Na_3VS_4 could index in tetragonal system with the space group $P\bar{4}21c$ (space group no. 114)[24] beside some impurities, such as V_2O_5, S. The XRD data of Na_3VS_4 was also analyzed with Rietveld refinement (Fig. 1b). The fitting was satisfactory with rather low factors of $R_{wp} \sim 4.98\%$ and $R_p \sim 3.61\%$. The cell parameters are $a = b = 13.5246(1)$ Å and $c = 7.9500(7)$ Å, with a unit volume of 1454.1(1) Å^3. According the Rietveld refinement results, the content of V_2O_5 and S was 2.62 wt% and 6.78 wt%, respectively. Detailed structural informations, including the atomic parameters determined from Rietveld refinement, were listed in Table 1. After P-doping, the $Na_3P_{0.1}V_{0.9}S_4$ sample could get a single phase (Fig. 1a), however, it exists a second phase of Na_3PS_4 in $Na_3P_{0.2}V_{0.8}S_4$ (Fig. 1a and d). This indicate that the solid-solution in $Na_3V_{1-x}P_xS_4$ was rather small. The Rietveld refinement of $Na_3P_{0.1}V_{0.9}S_4$ with tetragonal Na_3VS_4 structure model was shown in Fig. 1c. The refined profiles fitted well the observed data, which converged to $R_{wp} \sim 5.03\%$ and $R_p \sim 3.68\%$. The refined structural data and refinement parameters were listed in Table 2. The ratio of V/P is 0.88(5)/0.12(5) from the result of Rietveld refinement, which is agreed with the normal composition. The unit cell parameters obtained from the Rietveld refinement are $a = b = 13.5051(7)$ Å, $c = 7.9468(4)$ Å, $V = 1449.4(1)$ Å^3, which is a little less than those of Na_3VS_4. The compared cell parameters were given in Table 3. Due to the ionic radius of P^{5+} (0.29 Å)[11] is smaller than that of V^{5+} (0.46 Å),[25] P doping reduces the unit cell parameters.

Fig. 2 shows the Raman spectrum of Na_3VS_4 and $Na_3P_{0.1}V_{0.9}S_4$ at room temperature. The broad peak located at 450 cm^{-1} derived from the quartz box, and the peaks situated at about 490, 600 and 800 cm^{-1} could assign to the V–S or V/P–S vibrations of the isolated of VS_4^{3-} or V/PS_4^{3-} group, verifying the successful formation of VS_4^{3-} or V/PS_4^{3-} group.[12,20]

The crystal structure of tetragonal Na_3VS_4 viewed along *c* axes is given in Fig. 3a. The crystallographic structure unit cell can be simply described as consisting of isolated VS_4^{3-} tetrahedral groups separated by sodium cations. In unit cell, the Na1, Na2, Na3, Na4 atoms sit on 4d, 4c, 8e, 8e Wyckoff sites, V atoms locate at 8e sites and S atoms situate in 8e Wyckoff sites. The V–S distance are 2.38(1) Å (V–S1), 2.28 Å(1) (V–S2), 2.37(1) Å (V–S3), 2.36(1) Å (V–S4) and the S–V–S angles are 104.3° (S4–V–S1), 115.4° (S2–V–S1), 102.3° (S3–V–S2), 111.3° (S3–V–S4), 114.5° (S3–V–S1), 108.8° (S2–V–S4). In the crystal structure, Na atoms site on 4d (Na1), 4c (Na2), 8e (Na3), 8e (Na4) Wyckoff sites with different coordination environments (Fig. 3b), which are six-coordination for Na1, eight-coordination for Na2, six-coordination for Na3 and seven-coordination for Na4, respectively. Especially, Na2 atom connects to eight sulfur atoms and from an anion framework, all of these Na2 ion diffusion channels are constructed along mutually perpendicular paths (inset in the Fig. 3a). This anion framework is body-centered cubic

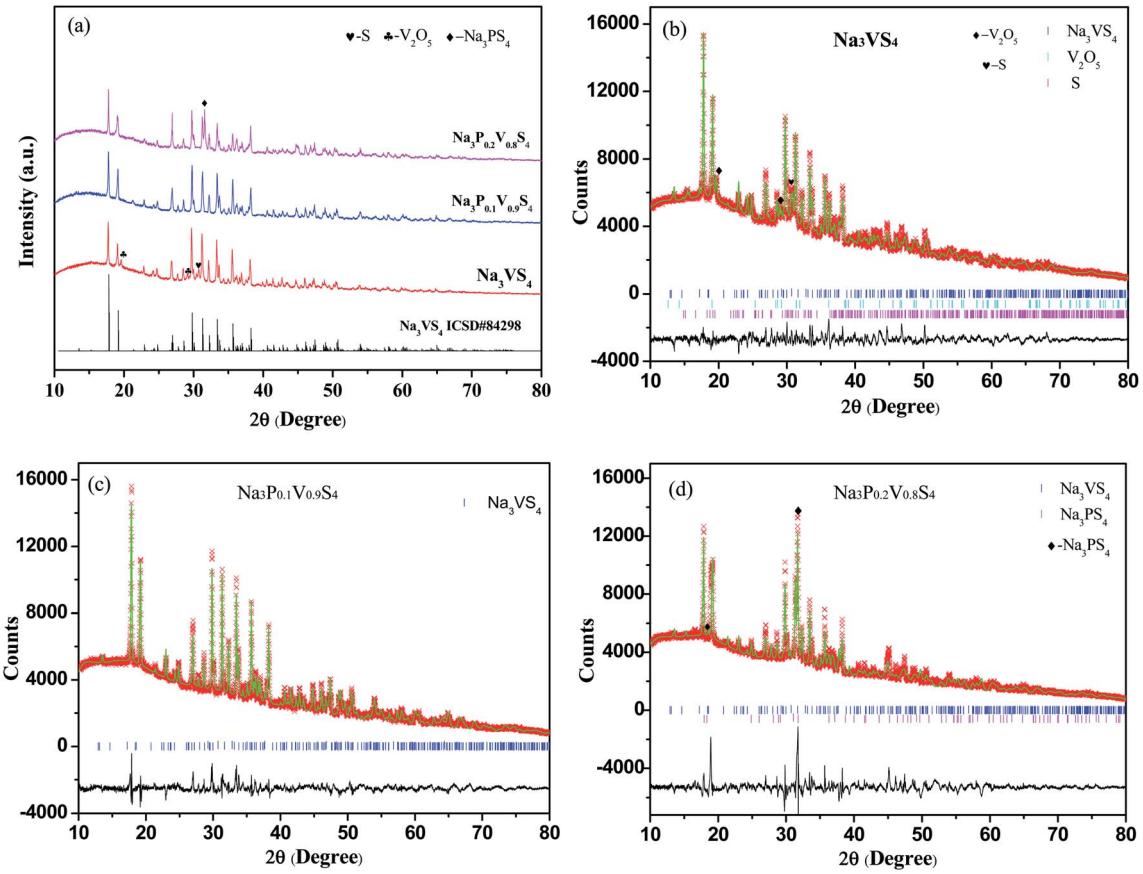

Fig. 1 (a) XRD patterns of $Na_3P_xV_{1-x}S_4$, ($0 \le x \le 0.2$) samples. (b) Rietveld refinement plots of XRD for tetragonal Na_3VS_4, the reliability factors are $R_{wp} = 4.98\%$ and $R_p = 3.61\%$. (c) Rietveld refinement plots of XRD for tetragonal $Na_3P_{0.1}V_{0.9}S_4$, the reliability factors are $R_{wp} = 5.03\%$ and $R_p = 3.68\%$. (d) Rietveld refinement plots of XRD for tetragonal $Na_3P_{0.2}V_{0.8}S_4$, the reliability factors are $R_{wp} = 7.79\%$ and $R_p = 5.18\%$.

framework, which benefits Na ion diffusion. This phenomenon similar to Gerbrand Ceder and co-workers proposed design principles for superionic conductors, they suggested that the body-centered cubic frameworks allow the migration of ions with a lower activation barrier than in other close-packed frameworks, thus resulting in fast ion diffusion.[26] Moreover, because of the ionic radius of P^{5+} less than the V^{5+}, the bond length of V/P–S is shorter than that of V–S (Fig. 3c). Also, as

Table 1 The final refined structural parameters of Na_3VS_4.[a]

Atom	Site	x	y	z	Occupancy	B_{iso} (Å^2)
Na1	4d	0	0.5	0.5314(26)	1	0.9(5)
Na2	4c	0.5	0.5	0.7260(29)	1	0.9(5)
Na3	8e	0.7528(13)	0.5468(10)	0.8531(16)	1	0.9(5)
Na4	8e	0.7544(13)	0.8004(9)	0.9030(20)	1	0.9(5)
V1	8e	0.0100(5)	0.7409(5)	0.7849(9)	1	2.6(2)
S1	8e	0.6806(7)	0.5051(9)	0.5262(12)	1	1.2(3)
S2	8e	0.8660(7)	0.6853(7)	0.6699(13)	1	1.2(3)
S3	8e	0.6069(7)	0.9049(8)	0.7042(15)	1	1.2(3)
S4	8e	0.5805(8)	0.6409(9)	0.8972(13)	1	1.2(3)

[a] Space group: $P\bar{4}21c$, $a = b = 13.5246(1)$ Å, $c = 7.9500(7)$ Å, $V = 1454.1(2)$ Å^3.

Table 2 The final refined structural parameters of $Na_3P_{0.1}V_{0.9}S_4$[a]

Atom	Site	x	y	z	Occupancy	B_{iso} (Å^2)
Na1	4d	0	0.5	0.5606(19)	1	1.7(2)
Na2	4c	0.5	0.5	0.7189(19)	0.92(3)	1.7(2)
Na3	8e	0.7580(9)	0.5477(7)	0.8339(13)	1	1.7(2)
Na4	8e	0.7577(9)	0.7970(7)	0.9361(15)	1	1.7(2)
V1/P1	8e	0.0101(3)	0.7347(3)	0.7811(5)	0.88(5)/0.12(5)	0.2(2)
S1	8e	0.6860(5)	0.5140(5)	0.5226(9)	1	0.8(1)
S2	8e	0.8748(5)	0.6877(5)	0.6752(10)	1	0.8(1)
S3	8e	0.6129(5)	0.8929(5)	0.6967(12)	1	0.8(1)
S4	8e	0.5744(6)	0.6609(6)	0.8843(8)	1	0.8(1)

[a] Space group: $P\bar{4}21c$, $a = b = 13.5051(5)$ Å, $c = 7.9467(4)$ Å, $V = 1449.5(1)$ Å^3.

comparing in Table 4, the average bond length of Na2–S in $Na_3V_{0.9}P_{0.1}S_4$ (3.60(6) Å) was larger than that of Na_3VS_4 (3.51(7) Å), indicating that sulfur anion channels in $Na_3P_{0.1}V_{0.9}S_4$ were

Table 3 The cell parameters of Na_3VS_4 and $Na_3P_{0.1}V_{0.9}S_4$

Composition	a/b (Å)	c (Å)	V (Å^3)
Na_3VS_4	13.5246(1)	7.9500(7)	1454.1(2)
$Na_3P_{0.1}V_{0.9}S_4$	13.5051(5)	7.9467(4)	1449.5(1)

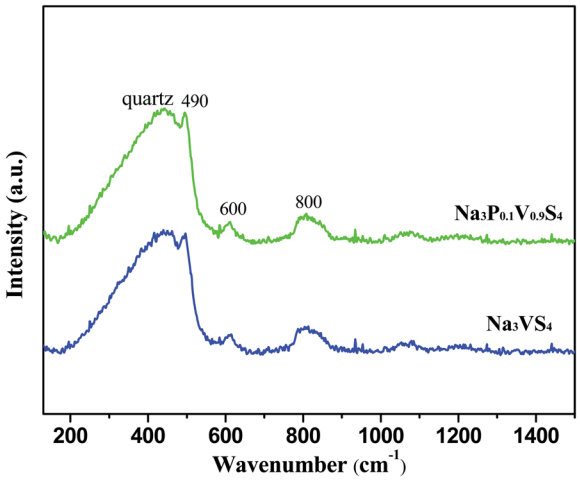

Fig. 2 Raman spectrum of Na_3VS_4 and $Na_3P_{0.1}V_{0.9}S_4$.

larger than the sulfur anion channels in Na_3VS_4. The larger channel reduced the force between sodium and sulfur, which is beneficial for Na ion diffusion.

Table 4 The bond length of Na2–S in Na_3VS_4 and $Na_3V_{0.9}P_{0.1}S_4$

Na_3VS_4	Length (Å)	$Na_3V_{0.9}P_{0.1}S_4$	Length (Å)
Na2–S1(×2)	3.15(1)	Na2–S1(×2)	3.25(1)
Na2–S1(×2)	2.91(1)	Na2–S1(×2)	2.98(1)
Na2–S4(×2)	2.58(1)	Na2–S4(×2)	2.69(1)
Na2–S4(×2)	5.41(1)	Na2–S4(×2)	5.48(1)
⟨*L*⟩	3.51(6)	⟨*L*⟩	3.60(7)

The conductivity of pressed pellets of Na_3VS_4 and $Na_3V_{0.9}P_{0.1}S_4$ were evaluated by AC impedance spectroscopy, which were conducted in the frequency range from 10^6 Hz to 0.1 Hz at 25–100 °C. The Nyquist plots of the impedance spectra of Na_3VS_4 and $Na_3P_{0.1}V_{0.9}S_4$ were shown in Fig. 4a and b, respectively. The impedance spectra both of Na_3VS_4 and $Na_3P_{0.1}V_{0.9}S_4$ contained a semicircle in the high-frequency region, which became smaller with increasing temperature. In the low frequency region, the semicircle segments follow a Warburg-type impedance,[27–29] which is associated with capacitive behavior and similar to the blocking electrodes.[30] The

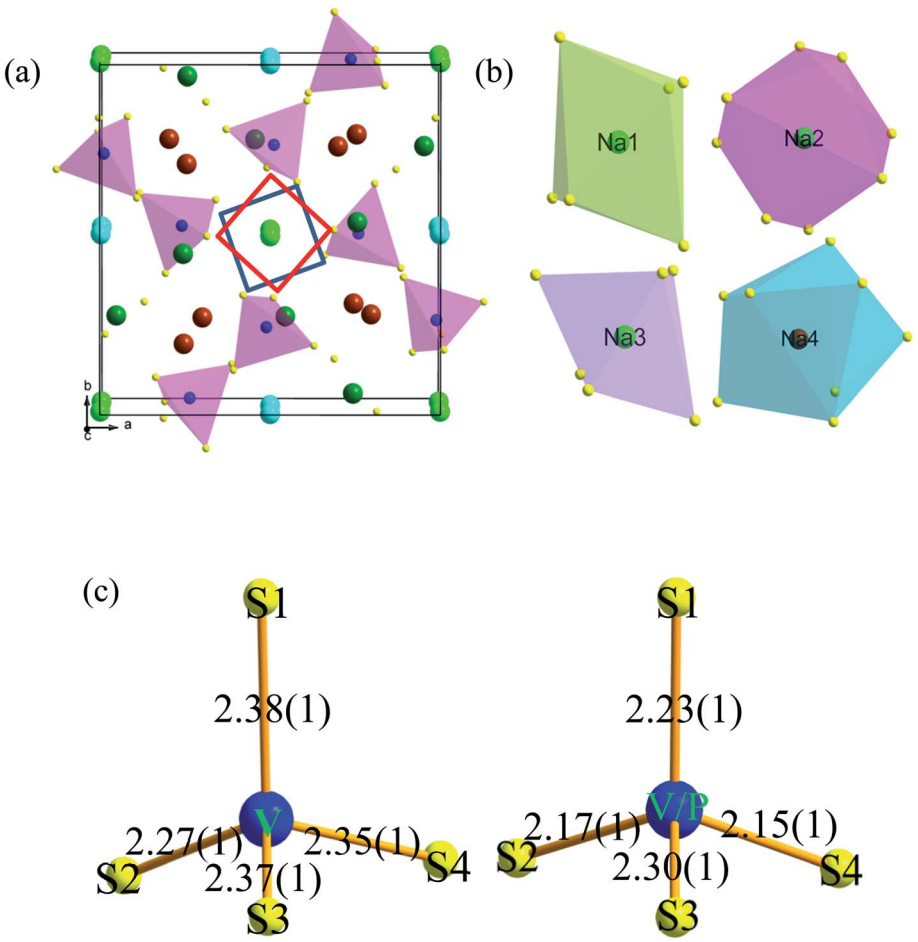

Fig. 3 (a) The crystal structure of Na_3VS_4 viewed along *c*, Na1 (turquoise), Na2 (bright green), Na3 (green), Na4 (brown), V (blue), S (yellow). (b) Na1 (turquoise), Na2 (bright green), Na3 (green), Na4 (brown) coordination environments. (c) Atomic and bond lengths of VS_4 and V/PS_4 polyhedron.

linear spike in the low-frequency region indicates Na_3VS_4 and $Na_3P_{0.1}V_{0.9}S_4$ were typical ionic conductor.

The Nyquist plot of $Na_3P_{0.1}V_{0.9}S_4$ at 25 °C (Fig. 4c) comprised bulk, grain boundary and electrode polarization. The high-frequency semicircle is characterized by a capacitance about 3×10^{-11} F cm^{-1} and could be attributed to ion transport in the crystalline and crystalline grains.[31] The electrode response was a Warburg-type spike characteristic of ion conductor. The total ionic conductivity (σ_t) could be calculated according to the formula:[31]

$$\sigma = R/(L \cdot S) \quad (1)$$

where R is the total resistance, which could be gained from the Nyquist plot, L is height of pellet, S is the contact area. Arrhenius plots of the total ionic conductivity σ for Na_3VS_4 and $Na_3P_{0.1}V_{0.9}S_4$ were depicted in Fig. 3d.

The linear dependence of $\log \sigma_t$ *versus* $(1/T)$ follows the Arrhenius law and indicates phase stability over the given temperature range. As show in the Table 5, the total ionic conductivity of Na_3VS_4 located in the range from 1.16×10^{-8} S cm^{-1} at 25 °C to 1.46×10^{-6} S cm^{-1} at 100 °C. However, the total ionic conductivity of $Na_3P_{0.1}V_{0.9}S_4$ placed 1.49×10^{-7} S cm^{-1} at 25 °C to 1.20×10^{-5} S cm^{-1} at 100 °C, which almost one order of magnitude higher than those of Na_3VS_4. The activation energy E_a for the sodium-ion conductor is determined from the slope of the linear Arrhenius plot using below equation:[32]

$$\sigma_t = A \exp(-E_a/k_B T) \quad (2)$$

where σ_t is the total ionic conductivity, A is the pre-exponential parameter, T is absolute temperature, E_a is the activation energy, and k_B is the Boltzmann constant. The calculated activation energy of Na_3VS_4 is 0.65 eV, while it is 0.54 eV for $Na_3P_{0.1}V_{0.9}S_4$. The lower activation energy of $Na_3P_{0.1}V_{0.9}S_4$ than that of Na_3VS_4 indicated that the diffusion rate of sodium ions in $Na_3P_{0.1}V_{0.9}S_4$ is higher than those of Na_3VS_4 leading to higher conductivity.

Compared with Na_3VS_4, the P-doping $Na_3P_{0.1}V_{0.9}S_4$ showed higher Na ionic conductivity. Through P substitution for V on $Na_3P_{0.1}V_{0.9}S_4$ composition, it could decrease the size of V/PS_4^{3-} tetrahedra and enlarge some sulfur anion channels. From the Rietveld refinement of $Na_3P_{0.1}V_{0.9}S_4$ data, the occupancy of Na2 sites contains 92% Na plus 8% vacancies rather than full occupancy of Na. Recently, theoretical investigations on both Na_3PS_4 (ref. 14) and Na_3PSe_4 (ref. 19) revealed that a defect-driven diffusion mechanism (either Na ion interstitial or Na

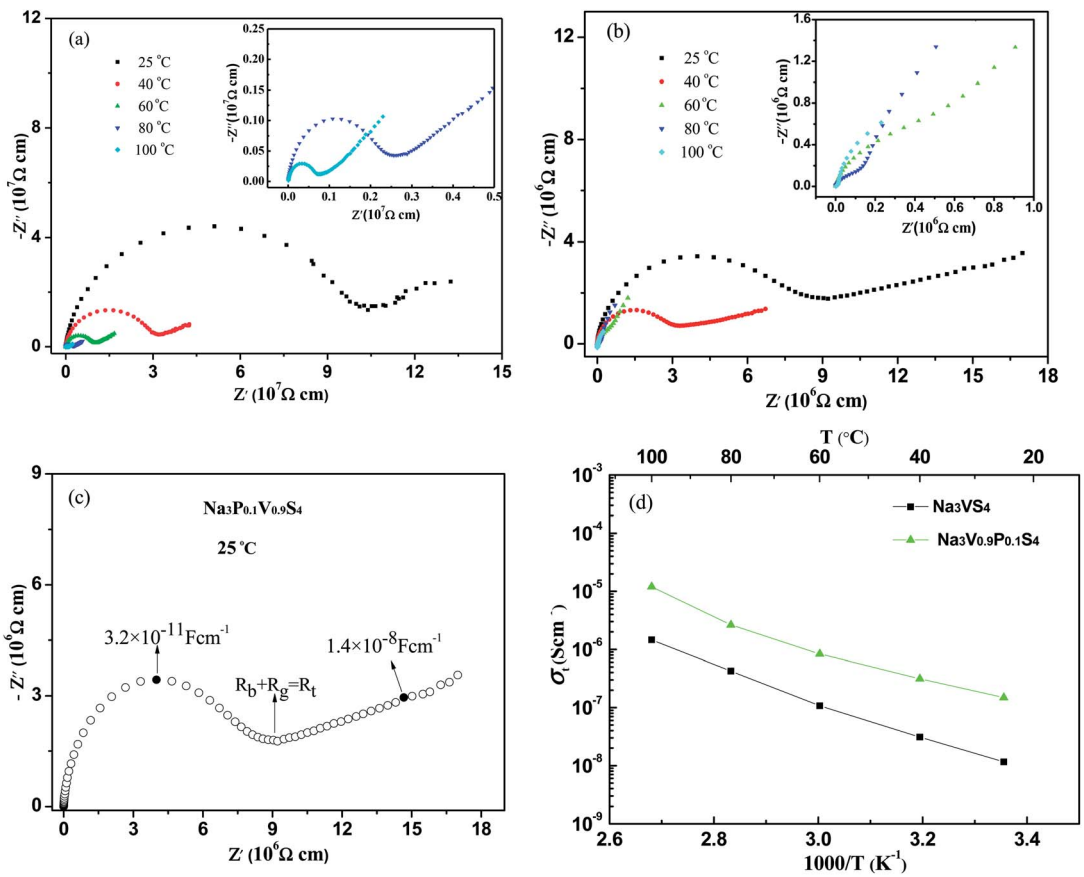

Fig. 4 (a) Nyquist impedance plot of Na_3VS_4 from 25 to 100 °C. (b) Nyquist impedance plot of $Na_3P_{0.1}V_{0.9}S_4$ from 25 to 100 °C. (c) Typical complex impedance plots of $Na_3P_{0.1}V_{0.9}S_4$ at 25 °C, R_b, R_g and R_t denote bulk, grain boundary and total resistivities, respectively. (d) Arrhenius conductivity plots of Na_3VS_4 and $Na_3P_{0.1}V_{0.9}S_4$ from 25 to 100 °C.

Table 5 Total ionic conductivity of Na_3VS_4 and $Na_3P_{0.1}V_{0.9}S_4$

Composition	25 °C (S cm^{-1})	40 °C (S cm^{-1})	60 °C (S cm^{-1})	80 °C (S cm^{-1})	100 °C (S cm^{-1})
Na_3VS_4	1.16×10^{-8}	3.11×10^{-8}	1.07×10^{-7}	4.23×10^{-7}	1.46×10^{-6}
$Na_3P_{0.1}V_{0.9}S_4$	1.49×10^{-7}	3.14×10^{-7}	8.30×10^{-7}	2.63×10^{-6}	1.20×10^{-5}

ion vacancy) accounts for the high ionic conductivity. Actually, Na ion deficiency is the reality during synthesis as it is a very reactive metal. Therefore, an ultrafast ion diffusion is expected if the conductor meets the prerequisites of sodium vacancy defects. In this work, these are about 8% of sodium vacancies in the Na2 position, therefore, these sodium vacancies are conducive to the diffusion of sodium ions. Benefit from these favorable features, P doping $Na_3V_{0.9}P_{0.1}S_4$ gets higher Na ion conductivity.

The total conductivity generally includes ionic conductors, minor electrons and/or holes ($\sigma_{(e+h)}$). Na_3VS_4 and $Na_3P_{0.1}V_{0.9}S_4$ total conductivity can be expressed by $\sigma_t = \sigma_{Na^+} + \sigma_{(e+h)}$. The transference number for sodium ions is accordingly derived by $t_{Na^+} = \sigma_{Na^+}/\sigma_t$.[20] To evaluate the exactly contribution of the electronic contribution to the total conductivity in the Na_3VS_4 and $Na_3P_{0.1}V_{0.9}S_4$ electrolytes, potentiostatic (0.5 V was used in the present work) DC measurements were carried out on Pt/Na_3VS_4/Pt and Pt/$Na_3P_{0.1}V_{0.9}S_4$/Pt cells at 25 °C. The electronic conductivity curves were displayed in Fig. 5a and b. When the measurement was performed, as there are no external sources for Na^+ ions, the electrodes are therefore blocking for Na^+ ions, and the conductivity at steady stage under a DC voltage could be ascribed to the electronic conduction. According to the chronoamperometric curves, the electronic resistance can calculate from the formula $R = U/I$ at steady stage, and then according to eqn (1) get the electronic conduction. The calculated values of $\sigma_{(e+h)}$ are about 8.60×10^{-9} and 1.76×10^{-8} S cm^{-1} for Na_3VS_4 and $Na_3P_{0.1}V_{0.9}S_4$, respectively. Therefore, the calculated transport number of sodium ions (t_{Na^+}) are about 0.3 for Na_3VS_4 and 0.9 for $Na_3P_{0.1}V_{0.9}S_4$ according to $t_{Na^+} = \sigma_{Na^+}/\sigma_t$, indicating that P-doing could greatly improve the transport number of sodium ions leading to higher total conductivity.

The electrochemical stability of Na_3VS_4 and $Na_3P_{0.1}V_{0.9}S_4$ with metallic sodium was estimated by using linear sweep voltammograms (LSV) on the Na/Na_3VS_4/Pt and Na/$Na_3P_{0.1}V_{0.9}S_4$/Pt cells,[33] as shown in Fig. 5c. Both of LSV curves do not appear apparent redox peak, indicating Na_3VS_4 and $Na_3P_{0.1}V_{0.9}S_4$ solid-state electrolytes exhibit a high electrochemical stability window up to 6 V.

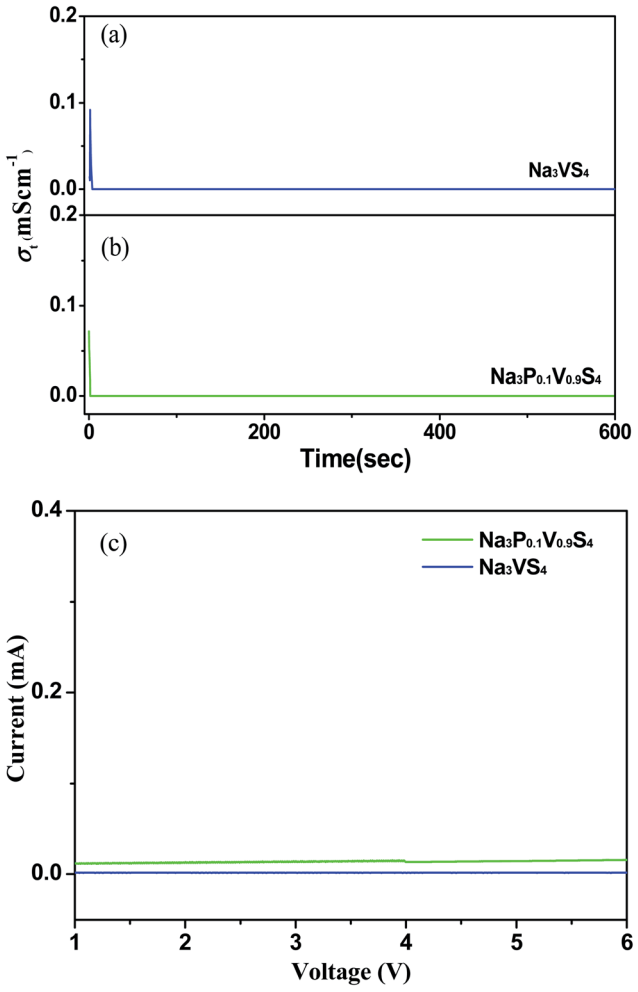

Fig. 5 Electronic conductivity curves for Na_3VS_4 (a) and $Na_3P_{0.1}V_{0.9}S_4$ (b), (c) LSV curves of Na_3VS_4 and $Na_3P_{0.1}V_{0.9}S_4$.

Conclusion

In summary, a new Na-ion solid-state electrolyte Na_3VS_4 with the space group $P\bar{4}21c$ was synthesized and investigated. Na1, Na2, Na3 and Na4 atoms locate at the 4d, 4c, 8e and 8e Wyckoff sites in the structure, respectively. Na2 atom sites bound to eight sulfur atoms and from a body-centered cubic anion framework, which is beneficial for Na ion diffusion. The total ionic conductivity of the parent composition Na_3VS_4 is $\sim 1.16 \times 10^{-8}$ to 1.46×10^{-6} S cm^{-1} from 25 to 100 °C. After substituting for V with P, the P-doping composition $Na_3P_{0.1}V_{0.9}S_4$, got the conductivity of 1.49×10^{-7} to 1.20×10^{-5} S cm^{-1} from 25 to 100 °C, which was higher than that of parent Na_3VS_4. The improvement of ion conductivity could ascribe to small P substitution for the large V giving rise to broaden the Na migration path and create of sodium vacancies. Also, both of Na_3VS_4 and $Na_3P_{0.1}V_{0.9}S_4$ solid-state electrolytes exhibit a high electrochemical stability window up to 6 V. This work will enrich the field of view sulfate-based sodium ion conductors and paves a new way to design new solid-state conductors for the next generation of solid-state Na ion batteries.

Conflicts of interest

There are no conflicts to declare.

Acknowledgements

The authors acknowledge the financial support of the National Natural Science Foundation of China (No. 21622101) and Guangxi Natural Science Foundation (No. 2017GXNSFBA198149).

References

1 D. Larcher and J. M. Tarascon, *Nat. Chem.*, 2015, **7**, 19–29.
2 H. Kim, Z. Ding, M. H. Lee, K. Lim and G. Yoon, *Adv. Energy Mater.*, 2016, **6**, 1600943.
3 X. B. Cheng, R. Zhang, C. Z. Zhao, F. Wei, J. G. Zhang and Q. Zhang, *Adv. Sci.*, 2016, **3**, 1500213.
4 H. Cheng, J. Liang and Z. Tao, *Adv. Mater.*, 2011, **23**, 1695–1715.
5 J. B. Goodenough and Y. Kim, *Chem. Mater.*, 2010, **22**, 587–603.
6 D. Bruce, K. Haresh and J. M. Tarascon, *Science*, 2011, **334**, 928–935.
7 J. J. Kim, K. Yoon, I. Park and K. Kang, *Small Methods*, 2017, **1**, 1700219.
8 J. Zhang, H. Wen, L. Yue, J. Chai, J. Ma and P. Hu, *Small*, 2017, **13**, 1–10.
9 K. Noriaki, H. Kenji, Y. Yuichiro, H. Masaaki, K. Ryoji and Y. Masao, *Nat. Mater.*, 2011, **10**, 682–686.
10 Y. Kato, S. Hori, T. Saito, K. Suzuki, M. Hirayama and A. Mitsui, *Nat. Energy*, 2016, **1**, 16030.
11 M. Jansen and U. Henseler, *J. Solid State Chem.*, 1992, **99**, 110–119.
12 A. Hayashi, K. Noi, A. Sakuda and M. Tatsumisago, *Nat. Commun.*, 2011, **3**, 856.
13 A. Hayashi, K. Noi, N. Tanibata, N. Motohiro and M. Tatsumisago, *J. Power Sources*, 2011, **258**, 420–423.
14 N. J. J. D. Klerk and M. Wagemaker, *Chem. Mater.*, 2016, **28**, 3122–3130.
15 K. Noi, A. Hayashi and M. Tatsumisago, *J. Power Sources*, 2014, **269**, 260–265.
16 N. Tanibata, K. Noi, A. Hayashi, N. Kitamura, Y. Idemoto and M. Tatsumisago, *ChemElectroChem*, 2014, **1**, 1130–1132.
17 N. Tanibata, K. Noi, A. Hayashi and M. Tatsumisago, *RSC Adv.*, 2014, **4**, 17120.
18 I. H. Chu, C. S. Kompella, N. Han, Z. Zhu, S. Hy and Z. Deng, *Sci. Rep.*, 2016, **6**, 33733.
19 L. Zhang, K. Yang, J. Mi, L. Lu, L. Zhao and L. Wang, *Adv. Energy Mater.*, 2015, **5**, 1501294.
20 L. Zhang, D. Zhang, K. Yang, X. Yan, L. Wang and J. Mi, *Adv. Sci.*, 2016, **3**, 1600089.
21 Z. Yu, S. Sl, S. Jh, D. Wang, X. Luo and Q. Huang, *Adv. Mater.*, 2017, **29**, 1605561.
22 M. Duchardt, U. Ruschewitz, S. Dehnen and B. Roling, *Angew. Chem., Int. Ed.*, 2018, **57**, 1351.
23 W. D. Richards, T. Tsujimura, L. J. Miara, Y. Wang, J. C. Kim and S. P. Ong, *Nat. Commun.*, 2016, **7**, 11009.
24 K. O. Klepp and G. Gabl, *Eur. J. Solid State Inorg. Chem.*, 1997, **34**, 1143–1154.
25 A. A. C. Coelho Software, Brisbane, Australia, 2005.
26 Y. Wang, W. D. Richards, S. P. Ong, L. J. Miara, J. C. Kim, Y. Mo and G. Ceder, *Nat. Mater.*, 2015, **14**, 1026.
27 P. Bron, S. Johansson, K. Zick, J. Schmedt auf der Günne, S. Dehnen and B. Roling, *J. Am. Chem. Soc.*, 2013, **135**, 15694–15697.
28 M. Tatsumisago, M. Nagao and A. Hayashi, *J. Asian Ceram. Soc.*, 2013, **1**, 17–25.
29 M. Duchardt, U. Ruschewitz, S. Dehnen and B. Roling, *Angew. Chem., Int. Ed.*, 2017, **57**, 1351–1355.
30 X. Feng, P. H. Chien, Z. Zhu, I. H. Chu, P. Wang, M. Immediato-Scuotto, H. Arabzadeh, S. P. Ong and Y. Y. Hu, *Adv. Funct. Mater.*, 2019, **29**, 1807951.
31 T. S. Irvine, C. Sinclair and A. R. West, *Adv. Mater.*, 1990, **2**, 132–138.
32 G. Sahu, L. Zhan, J. Li, Z. Liu and C. Liang, *Energy Environ. Sci.*, 2014, **7**, 1053–1058.
33 G. K. Kim, Y. J. Lim, H. Kim, Z. Liu and G. B. Cho, *Energy Environ. Sci.*, 2015, **8**, 3589–3596.

